

Using ion production to monitor the birth and death of a metastable helium Bose-Einstein condensate

S. Seidelin[§], O. Sirjean, J. Viana Gomes[†], D. Boiron, C. I. Westbrook and A. Aspect

Laboratoire Charles Fabry de l'Institut d'Optique, UMR 8501 du CNRS,
F-91403 Orsay Cedex, France

Abstract. We discuss observations of the ion flux from a cloud of trapped $2\ ^3S_1$ metastable helium atoms. Both Bose-Einstein condensates and thermal clouds were investigated. The ion flux is compared to time-of-flight observations of the expanded cloud. We show data concerning BEC formation and decay, as well as measurements of two- and three-body ionization rate constants. We also discuss possible improvements and extensions of our results.

PACS numbers: 34.50.-s, 67.65.+z, 03.30.Jp, 82.20.Pm, 05.30.-d

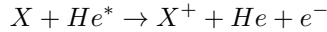
[§] To whom correspondence should be addressed (signe.seidelin@iota.u-psud.fr)

[†] Permanent address: Departamento de Fisica, Universidade do Minho, Campus de Gualtar, 4710-057 Braga, Portugal

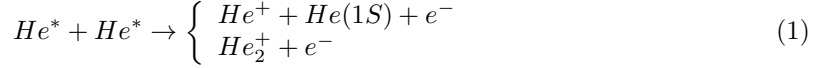
1. Introduction

Metastable helium (He^*), has recently joined the list of atomic species for which Bose-Einstein condensates (BEC) have been realized [1, 2]. Its major particularity is the 20 eV internal energy of the metastable state. Although this metastability leads to additional possible loss channels, it has been shown that these are not a serious problem. Indeed, ionizing collisions are a benefit because their low rate is nevertheless easily detectable. Ion detection is thus a new, “non-destructive” and real-time observation tool for studies of phenomenon of BEC formation kinetics [3, 4, 5, 6, 7]. In this paper we will describe our progress toward rendering quantitative the ion signal.

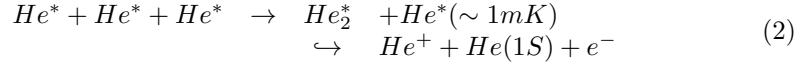
Several loss mechanisms are specific to the metastable state. First, collisions with the background gas lead to Penning ionization of the background gas:



The positive ion X^+ produced can be easily detected and if this is the dominant ion production mechanism as it is for a dilute sample (for a density $n \lesssim 10^{10} \text{ cm}^{-3}$), the corresponding flux is proportional to the number of trapped He^* atoms. So for example we can easily measure the lifetime of a dilute, trapped sample. This linearity no longer holds when the density of the trapped cloud becomes high. Collisions between atoms in the cloud must be taken into account. The relevant ionization mechanisms involve both two-body processes:



as well as a three-body process:



When these processes are present, the ion flux is related to the spatial integral of n^2 and n^3 . At BEC densities, the 2- and 3-body processes dominate the background gas ionization, and so detecting the ion flux in this case amounts to monitoring the atomic density.

In this paper, after a rapid description of our experimental setup, we present observations, via the ion flux, of the formation and the decay of a He^* BEC. The observations are mainly qualitative, but we discuss some of the requirements for making them quantitative. We then discuss our measurements of the 2- and 3-body ionization rate constants both in a BEC [8] and in a thermal cloud. We discuss some of the systematic errors in these measurements and conclude with some ideas for avoiding these errors.

2. Setup and experimental procedure

Our setup has been described previously [1, 8, 9]. Briefly, we trap up to 2×10^8 atoms at 1 mK in a Ioffe-Pritchard trap with a lifetime (τ) of 90 s. We use a “cloverleaf” configuration (Fig.1) [10] with a bias field $B_0 = 300 \text{ mG}$. The axial and radial oscillation frequencies in the harmonic trapping potential are typically $\nu_{\parallel} = 47 \pm 3 \text{ Hz}$ and $\nu_{\perp} = 1200 \pm 50 \text{ Hz}$ respectively ($\overline{\omega}/2\pi = (\nu_{\parallel}\nu_{\perp}^2)^{1/3} = 408 \text{ Hz}$). In

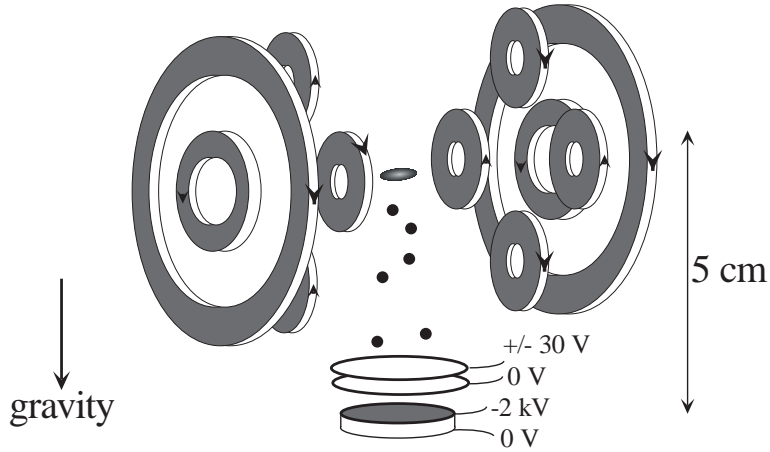


Figure 1. Experimental setup. The cold atoms are trapped in a cloverleaf type magnetic trap. A special feature of our set up is the microchannel plate detector (MCP) placed below the trapping region. Two grids above the MCP allow us either to repel positive ions and detect only the He^* atoms suddenly released from the trap (time-of-flight measurements), or to attract and detect the positive ions produced in the trapped cloud (ion rate measurements).

a typical run, forced evaporative cooling takes place for 40 s and is divided into 4 linear ramps. The last ramp lasts 5 seconds and the frequency decreases from 2000 kHz to a value between 1500 and 1000 kHz, depending on the condensed fraction wanted. A frequency of 1000 kHz (which is about 50 kHz above the minimum of the trapping potential) corresponds to the formation of a pure condensate.

A special feature of our set up is the detection scheme, based on a 2 stage, single anode microchannel plate detector (MCP) placed 5 cm below the trapping region (Fig.1). Two grids above the MCP allow us either to repel positive ions and detect only the He^* atoms, or to attract and detect positive ions produced in the trapped cloud. To detect the ion flux, the MCP is used in counting mode [8]: the anode pulses from each ion are amplified, and processed by a counter which records the time delay between successive events. We can also use the MCP to record a time-of-flight signal (TOF) of the atoms released from the trap. Because the width of the TOF distribution is small (about 5 ms for a BEC) compared to the mean arrival time (100 ms), all of the atoms hit the detector with nearly the same final velocity of 1 m/s. The TOF spectra are then proportional to the spatial distribution along the vertical direction, integrated over the two horizontal directions. To record the TOF we use the MCP in analog mode to avoid saturation due to a very high instantaneous flux [8].

3. Monitoring the evolution of a He^* cloud

To monitor the evolution of an atomic cloud, one usually releases the cloud and measures the TOF signal. Such a technique is destructive, and one must repeat the cooling sequence for each measurement. The TOF signals are thus subject to fluctuations in the initial number of atoms. In our case, we have a supplementary signal: the ion rate. We can thus minimize these fluctuations, by selecting runs having identical ion rates from the time between the beginning of the last rf-ramp until release.

Another type of observation is possible, however. We can use the evolution of the *value* of the ion rate, which is obtained in a single run, independent of any initial fluctuations. When the density is close to the density for BEC formation (i.e. $n \gtrsim 10^{12} \text{ cm}^{-3}$), 2- and 3-body collisions within the cloud dominate the ion production. Thus the ion rate is related to the density of the cloud via the 2- and 3-body rate constant. Under some conditions (see Appendix A) a record of the ion rate followed by a TOF measurement at the end of the formation of the BEC allows one to monitor the evolution of all the parameters of the cloud. In such an observation, knowledge of the 2- and 3-body rate constants is essential. This is the aim of the experiments described in section 4.

3.1. Observation of condensate formation during the evaporation ramp

Before trying to do a quantitative experiment on BEC formation out of a non-equilibrium uncondensed cloud [3, 4], we can explore qualitatively what happens during our standard evaporation ramp. We show in Fig. 2 the evolution of the ion rate from 2 seconds before the end of the rf-ramp to 2.5 seconds after it. In addition we show the TOF signals corresponding to various times before the end of the ramp, selected using their initial ion rate. Between times $t = -2$ s and $t = 0$, the rf-frequency was ramped down linearly from 1.4 MHz to 1 MHz. At $t = 0$ a pure condensate is formed. The comparison of the TOF and ion data first shows that the appearance of a narrow structure in the TOF spectrum corresponds, as closely as we can observe it, to an abrupt change in the slope of the ion signal. Thus, not only is the ion signal a reliable indicator of the presence of a BEC, but also a precise measure of the time of its appearance.

One's first reaction in looking at the ion rate signal is to assume that the higher the ion signal, the larger the BEC and the smaller the thermal cloud. Fig. 2 shows however, that this is not quite the case: the maximum in the ion signal arrives before the achievement of a pure BEC. In fact, computing the value of the ion signal is rather complex. First, as was discussed in Refs. [11, 12], as well as below, the indistinguishability of the atoms in the BEC renders the effective 2- and 3-body collision rate constants smaller than in the thermal cloud by factors of $1/2!$ and $1/3!$, respectively. Collisions between condensed and non-condensed atoms must also be taken into account [11] and the degree of overlap between the two clouds must be calculated. Thus it might be conceivable to see the ion rate go down when a BEC is formed. We show however in Appendix A that for a fixed total number of atoms, the ion rate monotonically increases as a BEC becomes more and more pure. The observation in Fig. 2 is explained by the fact that, up until $t = 0$ in Fig. 2, the atoms are being evaporatively cooled, as well as undergoing ionizing collisions and thus the total number of atoms must be decreasing. An explicit calculation including the atom

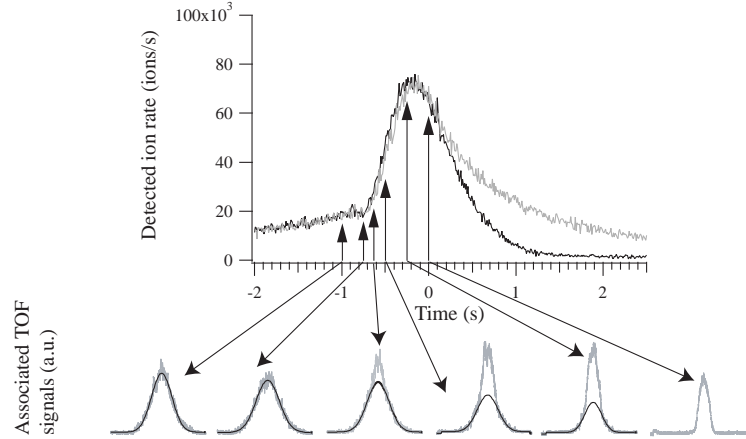


Figure 2. Single shot measurements of the ion rate versus time and the corresponding TOF signals. Forced evaporative cooling takes place until $t = 0$ (only the last 2 seconds of the RF-ramp are shown : from 1400 kHz to 1000 kHz). The arrows indicate the time the trap was switched off to record the TOF. The black curves superimposed on the TOF signals are Gaussian fits to the wings of the TOF. See also caption of Fig. 3.

loss is given in Appendix A and agrees qualitatively with our observations.

3.2. Observing the decay of the condensate

Figure 3 shows a series of TOF spectra taken after the end of the rf-ramp. Two situations are shown. In one case (grey ion curve) the rf-knife was held on at the frequency corresponding to the end of the ramp. In the other case (black ion curve) the rf-power was turned off completely at the end of the ramp. The data show that the condensate remains pure with the rf-knife kept on. In the absence of the rf-knife, the ion rate decays much faster and one sees that the sample rapidly acquires a thermal component. Since the total number of trapped atoms in the presence of a knife must be smaller than or equal to that in the absence of rf-knife, we conclude that the rapid decline in ion rate is due to a loss in sample density and not in the total number of atoms. This conclusion is confirmed by a fit to the thermal wings which reveals a heating as shown in Fig. 4.

3.3. Measuring the total number of atoms.

An attempt to measure the total number of atoms as a function of time is shown in Fig. 5. Both the total number and the condensed number as derived from fits to the TOF signals of Fig. 2 and Fig. 3 are plotted. Surprisingly the total number of atoms appears to increase between $t = 0$ and $t = 1$ s. There must be a systematic error, which we can account for by recalling that in our apparatus we only detect atoms which make non-adiabatic transitions to the (field insensitive) $m = 0$ state during the turn-off of the magnetic trap [1]. The fraction we observe is of order 10%. It is quite possible that this non-adiabatic transition does not occur with equal probability at every point in the trap. Thus clouds with different spatial distributions may be

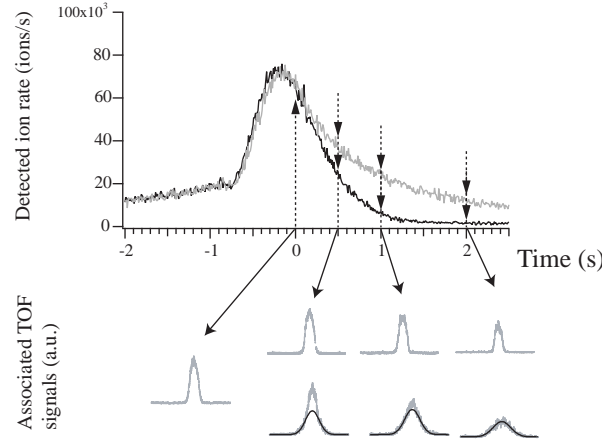


Figure 3. Same as the previous figure except that we examine the decay of the ion signal after $t = 0$. The upper TOF curves correspond to the upper (grey) ion decay curve (rf-shield present). The lower TOF curves correspond to the lower black ion curve (without rf-shield). This shows that the rf-shield is maintaining a quasi-pure BEC during the decay, and that in the absence of an rf-shield the condensate rapidly heats up, causing the ion rate to drop even faster.

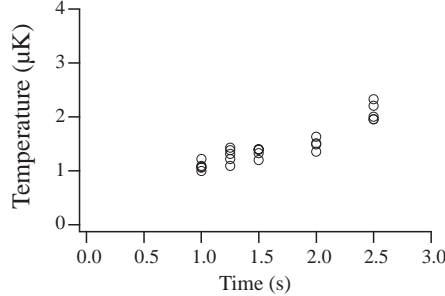


Figure 4. Heating of the condensate in the absence of an rf-shield. The temperature increases from $1.1 \mu\text{K}$ to $2.2 \mu\text{K}$ in 1.5 seconds. The time $t = 0$ is the same as in Fig. 2 and 3. For each different time, 4 different TOF's have been acquired and fitted.

converted to the $m = 0$ state with different efficiencies. This could explain why atoms in the thermal cloud are observed with a higher efficiency than condensed atoms, as indicated in Fig. 5.

We conclude that our measurements of the absolute number of atoms contain uncontrolled systematic errors of the order of a factor of two. So, even if we knew the ionization rate constants, we cannot use the ion rate to study condensate growth kinetics because we need the absolute value of the initial number of atoms and it would also be useful to measure the variation of the number of atoms during formation. Such a study will have to wait for a more reliable method of releasing the atoms from the trap (see conclusion). However, the measurement of the ionization rate constants is a first step. For a BEC, we can circumvent the systematic error on the detection efficiency

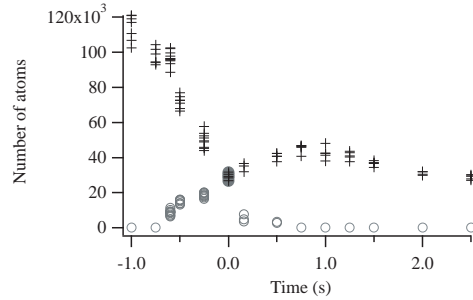


Figure 5. The measured number of atoms as a function of time. Crosses represent the total atom number, circles represent the number of atoms in the condensed part. The data comes from the fits of the TOF's presented in Fig. 2 and 3 and corresponds to the case where the rf knife is absent. The time scale indicated is the same as in Fig. 2 and 3. The increase in the total number after $t = 0$ is spurious (see text).

of the atoms to make a measurement of the ionization rate constants. This has been described in Ref. [8] and will be summarized in the following section. Afterwards, we will investigate the effect of this systematic error on the measurement for a thermal cloud.

4. Rate constants of ionizing collisions

The usual method of measuring the inelastic rate constants relies on fits to a non-exponential decay of the number of atoms. This method has some practical problems if the sample heats during the measurement: the density changes and complicates the fitting procedure. A way to avoid this heating is to apply an rf-shield, but this latter causes atom losses, which are not due to collisions. What is even more inconvenient in our case, is that what is measured in this kind of experiment is a decreasing atom number due to losses, which can be due to ionizing as well as non-ionizing collisions. We want to relate the ion rate to the density of the cloud, so what we need is the rate constants for *ionizing* 2- and 3-body collisions. We therefore use another method which consists in directly observing the products of the collisions, namely the number of ions, as a function of the density of the cloud.

As we have seen in section 3, there is a systematic error on the measurement of the number of atom and so of the density of the cloud. But we will see that we can circumvent it in the case of the BEC. Let us then assume in a first part that we are able to measure accurately the number of atoms.

We use the MCP to detect both the ions and the TOF signal. In a single run we record the ion rate during the last seconds of the ramp until we switch off the magnetic trap and record the TOF signal (to obtain the atom number N and the density). The very last value of the ion rate recorded corresponds to ions produced by the cloud observed with the TOF signal. We repeat this sequence many times with different numbers of atoms in the cloud. The way to vary this number is to keep the atoms in the trap with an rf-shield kept on. In this way we reduce the atom number and keep the temperature of the cloud constant. As explained in Appendix A, the relation between ion rate and density is quite complex in the case of the presence of

collisions between atoms in the condensed part and atoms in the thermal part. We therefore only examine the case of a pure BEC or a pure thermal cloud. In that case we can write the ion rate per atom Γ as follows

$$\frac{\text{ion rate}}{N} = \Gamma = \frac{1}{\tau'} + \frac{1}{2} \kappa_2 \beta \langle n \rangle + \frac{1}{3} \kappa_3 L \langle n^2 \rangle. \quad (3)$$

where $\langle n \rangle = \frac{1}{N} \int n^2 d\mathbf{r}$ and $\langle n^2 \rangle = \frac{1}{N} \int n^3 d\mathbf{r}$, n being the local density. We have also introduced the 2-body and 3-body ionizing collision rate constants, β and L , respectively, defined according to their effect on the density loss in a thermal gas [13]: $(\frac{dn}{dt})_{\text{ionization}} = -\frac{n}{\tau'} - \beta n^2 - L n^3$. The effective lifetime $\tau' \geq \tau$ is due to *ionizing* collisions with the background gas. The numerical factors come from the fact that although 2 or 3 atoms are lost in each type of collision, only 1 ion is produced. The factors κ_2 and κ_3 take into account the fact that the 2 and 3-particle local correlation functions are different depending on whether it is a BEC or a thermal cloud. For the thermal cloud $\kappa_2 = \kappa_3 = 1$, while for a dilute BEC, one has $\kappa_2 = 1/2!$ and $\kappa_3 = 1/3!$ [11, 12]. When the sample is very dense, quantum depletion must be taken into account, which modifies these factors [11]. A measurement of β and L would allow us to test experimentally the theoretical values of κ_2 and κ_3 [8].

4.1. Rate constants for a BEC

To determine the ionizing collision rate constants β and L , we need an absolute calibration of the number of atoms in the condensate N_0 , and the peak density n_0 in order to calculate $\langle n \rangle$ and $\langle n^2 \rangle$. As discussed above, we do not have a good calibration of these quantities. In the case of a BEC however, the measurement of the chemical potential μ obtained by a fit of the TOF signal, gives an accurate value for the product $n_0 a = \mu m / 4\pi\hbar^2$, a being the scattering length. With the value of $\bar{\omega}$ we also obtain the product $N_0 a = (1/15) (\hbar/m\bar{\omega})^{1/2} (2\mu/\hbar\bar{\omega})^{5/2}$. Experimentally we confirm that $\mu \propto N_d^{2/5}$ where N_d is the number of detected atoms [8]. This is a good indication that our detector is linear and that the detection efficiency for a BEC is indeed independent of μ . Assuming a value of the scattering length ($a = 20$ nm), we have therefore an accurate measurement of n_0 and N_0 . We have measured the rate constants β and L for a condensate [8]. We obtain by a fit to equation (3) (having corrected for the effect of quantum depletion and the fact that the BEC also contains a small thermal fraction) $\beta = 2.9(\pm 2.0) \times 10^{-14} \text{ cm}^3 \text{ sec}^{-1}$ and $L = 1.2(\pm 0.7) \times 10^{-26} \text{ cm}^6 \text{ sec}^{-1}$. These values agree with the theoretical estimates [14, 15]. The scattering length is not well-known [1, 2], so we have also given β and L for different values of a [8].

4.2. Rate constants for a thermal cloud

To determine the rate constants for a thermal cloud we need, as before, to determine the atom number and density. We cannot use the same trick as in section 4.1 to avoid systematic errors in the detection efficiency. If we want to use the above experimental method for a thermal cloud we must rely on a fit of the TOF to find the atom number and the temperature T . In Appendix B, we propose a method to determine the rate constants which is independent of an absolute detection efficiency, but at this stage we will concentrate on the same technique as used for a BEC.

As we have shown above, the detection efficiency is expected to be different for a thermal cloud and we can investigate the effect of this systematic error on these

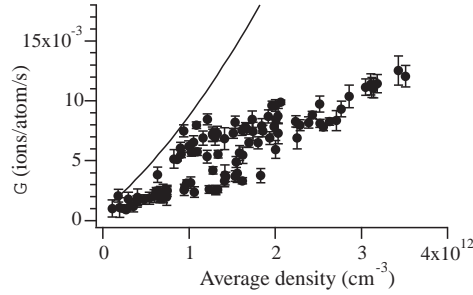


Figure 6. Ion rate per trapped atom (Γ) in a thermal cloud versus average density. The solid curve corresponds to the value of β and L deduced from the condensate measurements.

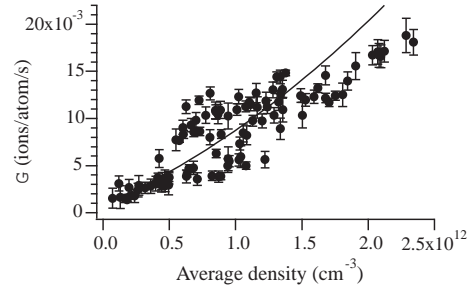


Figure 7. Same as Fig. 6 but assuming a factor of 1.5 higher detection efficiency of the thermal cloud relative to the BEC. The data have simply been re-scaled along both axes; the solid curve is the same as in Fig. 6.

measurements. We repeat the above described experiment, this time with a pure thermal cloud. To begin with, we assume that the detection efficiency is the same for a BEC and a thermal cloud. We plot the ion rate per atom as a function of $\langle n \rangle$ in Fig. 6. We can extrapolate the data to obtain the vertical intercept, which corresponds to $1/\tau'$. For densities corresponding to the moment of formation of BEC, the corresponding ion rate N/τ' is negligible compared to the total ionization rate, meaning that we are dominated by 2- and 3-body processes (see Fig. 2 and 5). To compare with the results obtained for the BEC, we have also plotted the curve we would expect using the above values of β and L . It is clear that the data do not agree with this curve. Moreover, no possible pair of β and L taken within their error bars (see [8]) can transform the curve so that it agrees with the data. Nor can assuming a different scattering length. What *can* make the curve agree with the data is assuming a different detection efficiency for atoms in the thermal cloud. If we assume for example that the detection efficiency is a factor of 1.5 higher for a thermal cloud relative to a BEC (which is consistent with Fig. 5), the curve agrees better with the data as shown in Fig. 7.

The dispersion of the data points is quite large. This dispersion can be understood by examining Fig. 8 in which we have plotted the same data as in Fig. 6, but now indicating the temperature corresponding to each different point on the graph. There

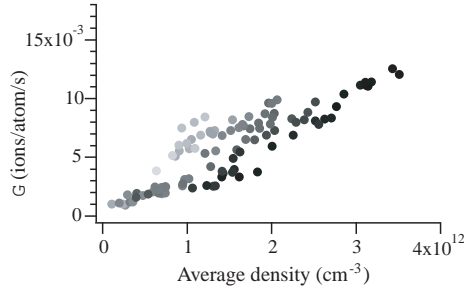


Figure 8. Same data as in Fig. 6 but with the different temperatures indicated. The light grey corresponds to the point with higher temperatures (the maximum temperature is $5.5 \mu K$), the black points with lower temperatures (minimum temperature $1.8 \mu K$).

is a clear systematic variation with temperature. One possible explanation is that the detection efficiency is temperature dependent. This agrees with the above idea that the efficiency depends on the spatial extent of the cloud which is indeed related to the temperature. We do not know the form of the detection efficiency as a function of temperature, but comparing these data (indicating that cold atoms are better detected) with the fact that a thermal cloud is better detected than a BEC, leads us to conclude that there exists a certain temperature giving a maximal detection efficiency. Therefore the correction to the detection efficiency for thermal atoms is not just a simple factor, but rather a function of temperature. Without knowing this correction, we cannot use this method to determine the collision constants for a thermal cloud. Still, these results are a consistency check on the rate constants measured using a BEC.

5. Conclusion

We have seen that the benefits of ion detection are twofold. First, the ion rate can be used to select BECs' with very similar parameters out of a sample with large fluctuations. Second, the ion rate itself can give information on the condensate on a single shot basis. Quantitatively, we still have some difficulties interpreting the data due to systematic errors in the detection calibration.

One way to overcome this problem is to release the atoms from the trap by the mean of Raman transitions. It should be possible to transfer close to 100% of the atoms into the $m = 0$ state. This will eliminate the temperature dependence of the detection efficiency and allow us to obtain more precise measurements of β and L , both for the BEC by improving the value of the scattering length and for the thermal cloud by making the detection efficiency temperature independent.

6. Acknowledgements

We thank A. Villing and F. Moron for their assistance with the electronics. This work is supported by the European Union under grants IST-1999-11055 and HPRN-CT-2000-00125, and by the DGA grant 00.34.025. J.V.G. thanks Fundação para a

Ciênci a Tecnologia and S.S. acknowledges Danish Research Training Council and Danish Research Agency for financial support.

Appendix A. Predictions of the ion rate during the formation of the BEC

The 2- and 3-body ion rates (I_{2b} and I_{3b} , respectively) in a sample containing both a BEC and a thermal cloud is given by [11]:

$$I_{2b} = \frac{\beta}{2!} \int d\mathbf{r} [n_0^2(\mathbf{r}) + 4n_0(\mathbf{r})n_{th}(\mathbf{r}) + 2n_{th}^2(\mathbf{r})] \quad (\text{A.1})$$

$$I_{3b} = \frac{L}{3!} \int d\mathbf{r} [n_0^3(\mathbf{r}) + 9n_0^2(\mathbf{r})n_{th}(\mathbf{r}) + 18n_0(\mathbf{r})n_{th}^2(\mathbf{r}) + 6n_{th}^3(\mathbf{r})] \quad (\text{A.2})$$

where $n_0(\mathbf{r})$ is the local density of the BEC and $n_{th}(\mathbf{r})$ is the local density of the thermal cloud. Here we have taken into account the symmetrization factors, but neglected quantum depletion.

Four parameters are needed to determine the densities of the two clouds : N_0 , μ , N_{th} and T_{th} . In the Thomas-Fermi approximation however, the BEC density depends only on μ :

$$n_0(\mathbf{r}) = \max \left[0, \frac{\mu - U(\mathbf{r})}{g} \right] \quad (\text{A.3})$$

with $U(\mathbf{r})$ the harmonic trapping potential and $g = \frac{4\pi\hbar^2 a}{m}$ the interaction strength. The density of the thermal cloud depends on two parameters. But, if thermodynamic equilibrium is reached, taking into account the interactions between the BEC and the thermal cloud (and neglecting the interaction energy of the thermal cloud), we can write:

$$n_{th}(\mathbf{r}) = \frac{1}{\lambda_{dB}^3} g_{3/2} \left(\exp^{-\frac{1}{k_B T}(U(\mathbf{r}) + 2g n_0(\mathbf{r}) - \mu)} \right) \quad (\text{A.4})$$

where λ_{dB} is the thermal de Broglie wavelength and $g_{3/2}(x) = \sum_{n=1}^{+\infty} \frac{x^n}{n^{3/2}}$. In that case, given μ , n_{th} only depends on one additional parameter.

Appendix A.1. Comparison on the ion rates created by a thermal cloud at $T = T_C$ and a pure BEC

Before trying to calculate the ion rate for any T , which requires numerical calculation, let us first examine the ion rate created by a thermal cloud at $T = T_C$ with a number of atoms N and that created by a pure BEC ($T = 0$) with a number of atoms ηN ($\eta < 1$).

In the case of 2-body collisions, the ratio R_{2b} of the ion rates created by a pure BEC (I^{BEC}) and by a thermal cloud (I^{th}) is related to the ratio of the peak densities. For 3-body collisions the ratio (R_{3b}) is related to the square of that ratio. Using the above equations we find:

$$\left(\frac{n_0}{n_{th}} \right) = C_0 \times \eta^{2/5} \times N^{-1/10} \left(\frac{\bar{\sigma}}{a} \right)^{3/5} \quad (\text{A.5})$$

$$R_{2b} = \frac{I_{2b}^{BEC}}{I_{2b}^{th}} = C_2 \times \eta^{7/5} \times N^{-1/10} \left(\frac{\bar{\sigma}}{a} \right)^{3/5} \quad (\text{A.6})$$

$$R_{3b} = \frac{I_{3b}^{BEC}}{I_{3b}^{th}} = C_3 \times \eta^{9/7} \times N^{-2/10} \left(\frac{\bar{\sigma}}{a} \right)^{6/5} \quad (\text{A.7})$$

where $\bar{\sigma} = \sqrt{\frac{\hbar}{m\bar{\omega}}}$. The numerical factors $C_0 \simeq 0.78$, $C_2 \simeq 1.05$ and $C_3 \simeq 0.49$ are independent of the atom considered and only assume that the cloud is trapped in a 3D harmonic trap. The maximum ratios are reached in the case of no loss ($\eta = 1$). Using the typical values of our experiment ($a \simeq 20$ nm, $N \simeq 4. \times 10^5$, and $\bar{\omega} \simeq 2\pi \times 408$ Hz), we find $\left(\frac{n_0}{n_{th}} \right)_{max} \simeq 4$, $(R_{2b})_{max} \simeq 5$ and $(R_{3b})_{max} \simeq 12$.

If the total number of atoms decreases during the formation of the BEC, these ratios rapidly fall. For instance, if the number of atoms decreases by a factor of 3.5 during the last 750 ms of evaporation as shown in Fig. 5, we would not have seen an increase of ionization rate but roughly the same ion rate at $t = -750$ ms and at $t = 0$ ms ! This is an additional evidence of the difference of neutral atom detection efficiency for a thermal cloud and BEC (i.e. the total number of atoms decreased by less than 3.5).

Appendix A.2. Evolution of the ion rate between $T = T_C$ and $T = 0$

Using equation (A.1) and (A.2), we have numerically calculated the ion rates for all temperatures. If the cloud is at thermodynamic equilibrium all the parameters of the cloud are deduced from 2 parameters, for example the total number of atoms and the temperature. To simulate a time evolution of the ion rate we thus need a model for the variation of these parameters. In this appendix we will assume a linear evolution of the temperature between $T = T_C$ and $T = 0$ in 0.7 sec. This is of course a simplification, but given the linearity of the evaporative cooling ramp, it is a quite good approximation.

In Fig. A1 a) we show the evolution of the ion rates assuming a constant total number of atoms. The ion rate increases monotonically. We also see that the number of ions produced and thus also the number of lost atoms is not necessarily negligible compared to the total.

We can attempt to take into account these losses in our model. In the experiments described in the text, the losses are not only due to the ionizing collisions but also to the rf-knife. In addition, losses not only lead to a decrease of the total number of atoms but also to a change of the temperature because these collisions change the condensed fraction. Thus, modelling the ion rate can be quite complicated. Here we wish simply to illustrate the effect of loss, so we assume that losses are only due to ionizing collisions, and we will neglect losses due to the rf-knife. Figure A1 b) shows the results. The atom number decreases by only 30 % and the ion rate reaches a local maximum before the formation of the pure BEC, as in our experiment. Extensions of our model to include losses due to the rf-knife would allow one to monitor all the parameters of the cloud using the ion signal.

Appendix B. Proposed measurement of rate constants independent of absolute neutral atom detection efficiency

We will assume in this section that the absolute ion detection efficiency is known, and that 2- and 3-body losses are ionizing collisions [14]. The idea behind this method is that two TOF signals separated by a given time can measure the relative atom loss

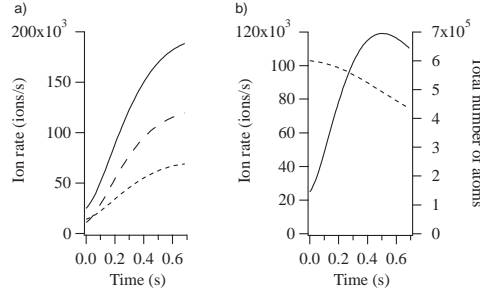


Figure A1. Evolution of the ion rate with time. In a) the total number of atoms is constant. We show the different contributions to the total ion rate (continuous curve) of the ion rate created by 2-body collisions (short dashed curve) and 3-body collisions (long dashed curve.) In b) the total number of atoms (dashed curve) decrease with the only effect of ionizing collisions. Here the ion rate exhibits a maximum before the formation of a pure BEC. For both graphs, the initial number of atoms is 6×10^5 and a linear evolution of the temperature between T_C and 0 is imposed. The rates have been calculated with the values of rate constants measured in [8].

during this time, while the ion rate can measure the absolute atom loss. These data allow one to extract the rate constants without relying on an absolute calibration of the neutral atom detection efficiency. The method works if the neutral detection efficiency is unknown, but independent of temperature. Otherwise, we must also assume that the cloud does not heat during the measurement or that we know the variation of detection efficiency with temperature.

To simplify the discussion we will neglect 3-body reactions and assume that the sample does not heat during the measurement. This will allow us to derive analytical expressions, but the results are easily generalized to include heating as well as 3-body reactions. We can then write the ion rate $I(t)$ as:

$$I(t) = \frac{\epsilon N(t)}{\tau'} + \frac{\beta \epsilon}{2V_{eff}} N(t)^2 \quad (\text{B.1})$$

with τ' the life time due to ionizing collisions, $N(t)$ the absolute atom number, V_{eff} defined by $\langle n \rangle = \frac{N}{V_{eff}}$ and ϵ the ion detection efficiency. We write $N_d(t) = \alpha N(t)$ where $N_d(t)$ is the detected number of atoms, and α is the neutral atom detection efficiency. Then

$$I(t) = \frac{\epsilon N_d(t)}{\alpha \tau'} + \frac{\epsilon \beta}{\alpha^2 2V_{eff}} N_d(t)^2 \quad (\text{B.2})$$

We can also write an equation for the atom number

$$\frac{dN(t)}{dt} = -\frac{N(t)}{\tau} - \frac{\beta}{V_{eff}} N(t)^2 \quad (\text{B.3})$$

with τ the total life time of the sample that we can measure independently at lowest density. The solution is:

$$\frac{N(t)}{N(t_0)} = \frac{1}{(1 + \frac{\beta}{V_{eff}} N(t_0) \tau) e^{(t-t_0)/\tau} - \frac{\beta}{V_{eff}} N(t_0) \tau} \quad (\text{B.4})$$

substituting again $N_d(t) = \alpha N(t)$ we have:

$$\frac{N_d(t)}{N_d(t_0)} = \frac{1}{(1 + \frac{\beta}{\alpha V_{eff}} N_d(t_0) \tau) e^{(t-t_0)/\tau} - \frac{\beta}{\alpha V_{eff}} N_d(t_0) \tau}} \quad (\text{B.5})$$

Thus we can measure an initial ion rate and the corresponding detected atom number $N_d(t_0)$ by a TOF signal, let the system evolve during a certain time and then again measure the ion rate and the atom number $N_d(t)$. With the evolution of the ion rate, we can deduce $\epsilon/\alpha\tau'$ and $\frac{\epsilon\beta}{\alpha^2 V_{eff}}$ from equation (B.1), and from the evolution of the atom number we can deduce $\frac{\beta}{\alpha V_{eff}}$ using equation (B.5). With the value of V_{eff} and ϵ , we can obtain the value β . We can also obtain the detection efficiency α .

If we allow for three-body reactions, the method can still be used but (B.4) is no longer analytical and must be integrated numerically. If the sample heats during the measurement, we only have to recalculate the volume V_{eff} for each TOF measurement.

The reason why we have yet not been able to apply this method is as indicated above that the sample is heating so that the detection efficiency changes during the measurement. As we have not been able to measure the temperature dependence of $\alpha(T)$ the above equations cannot be solved. We hope to render the detection efficiency temperature independent in the near future by using Raman transitions as mentioned in the conclusion.

- [1] Robert A, Sirjean O, Browaeys A, Poupart J, Nowak S, Boiron D, Westbrook C I and Aspect A 2001 *Science* **292**, 461.
- [2] Pereira Dos Santos F, Lonard J, Junmin Wang, Barrelet C J, Perales F, Rasel E, Unnikrishnan C S, Leduc M and Cohen-Tannoudji C 2001 *Phys. Rev. Lett.* **86**, 3459.
- [3] Miesner H J, Stamper-Kurn D M, Andrews M R, Durfee D S, Inouye S and Ketterle W 1998 *Science*, **270**, 1005.
- [4] Köhl M, Hänsch T W and Esslinger T 2002 *Phys. Rev. Lett.* **88**, 080402.
- [5] Kagan Yu M, Svistunov B V and Shlyapnikov G V 1992 *Sov. Phys. JETP* **75**, 387.
- [6] Gardiner C W, Zoller P, Ballagh R J and Davis M J 1997 *Phys. Rev. Lett.* **79**, 1793.
- [7] Bijlsma M J, Zaremba E and Stoof H T C 2000 *Phys. Rev. A* **62**, 063609-1.
- [8] Sirjean O, Seidelin S, Viana Gomes J, Boiron D, Westbrook C I and Aspect A, Accepted for publication in *Phys. Rev. Lett.*
- [9] Browaeys A, Thèse de l'université Paris-Sud (2000), available at <http://ccsd.cnrs.fr/>.
- [10] Mewes M O, Andrews M R, van Druten N J, Kurn D M, Durfee D S and Ketterle W 1996 *Phys. Rev. Lett.* **77**, 416.
- [11] Kagan Yu M, Svistunov B V and Shlyapnikov G V 1985 *JETP Lett.* **42**, 209.
- [12] Burt E A, Ghrist R W, Myatt C J, Holland M J, Cornell E A and Wieman C E 1997 *Phys. Rev. Lett.* **79**, 337.
- [13] Collision rate constants are sometimes defined directly for a BEC ($\beta' = \beta/2$ and $L' = L/6$).
- [14] Shlyapnikov G V, Walraven J T M, Rahmanov U M and Reynolds M W 1994 *Phys. Rev. Lett.* **73**, 3247; Fedichev P O, Reynolds M W, Rahmanov U M and Shlyapnikov G V 1996 *Phys. Rev. A* **53**, 1447.
- [15] Venturi V, Whittingham I B, Leo P J and Peach G 1999 *Phys. Rev. A* **60**, 4635; Venturi V and Whittingham I B 2000 *Phys. Rev. A* **61**, 060703(R).